Research Article

Mohamed S. Kamar, Ibrahim A. Salem, Ibrahim E. El-Aassy, Abdu A. El-Sayed, Hamdy A. Awad*, Huseyin Ozan Tekin*, Abdullah M. Alzahrai, El Saeed R. Lasheen

Petrology and geochemistry of multiphase post-granitic dikes: A case study from the Gabal Serbal area, Southwestern Sinai, Egypt

https://doi.org/10.1515/chem-2022-0136
received January 15, 2022; accepted February 2, 2022

Abstract: Variable single and/or swarms of post-granitic dikes are widespread at Gabal Serbal, Southwestern Sinai, Egypt. The present article aims to identify and discriminate these multiphase dikes through detailed geological, petrographical, and geochemical examinations. These dikes are classified into two subphases: (1) acidic dikes (porphyritic dacite, microgranite, granophyre, and alkaline granophyre dikes); and (2) basic dikes (basalt and dolerite dikes). They range from vertical or steeply inclined bodies, 0.5–15 m wide, pink to black color, and NE–SW to N–S directions. Acidic dikes with different mineralogical constituents have medium to high *k*-characters, originating from calc-alkaline magma and extruded in a volcanic arc environment. In contrast, basic dikes have medium *k*-characters, originating from tholeiitic magma and developing within a plate environment. Basic dikes are enriched with opaque minerals, where the basaltic dike contains iron oxides (magnetite and hematite), such as apatite in addition to copper minerals. Dolerite dike comprises magnetite, titanomagnetite, and pyrite.

Keywords: dikes, Gabal Serbal, geochemistry, Sinai, Egypt

*** Corresponding author: Hamdy A. Awad,** Institute of Earth Sciences, Southern Federal University, 40 Zorge St., 344090 Rostov-on-Don, Russia; Geology Department, Faculty of Science, Al-Azhar University, Assuit Branch, 71524 Assuit, Egypt, e-mail: hamdiawaad@gmail.com
*** Corresponding author: Huseyin Ozan Tekin,** Department of Medical Diagnostic Imaging, College of Health Sciences, University of Sharjah, 27272, Sharjah, United Arab Emirates; Istinye University, Faculty of Engineering and Natural Sciences, Computer Engineering Department, Istanbul 34396, Turkey, e-mail: tekin765@gmail.com
Mohamed S. Kamar: Nuclear Materials Authority, P.O. Box 530 El Maadi, Cairo, Egypt, e-mail: drkamar30@gmail.com
Ibrahim A. Salem: Geology Department, Faculty of Science, Tanta University, Tanta, Egypt, e-mail: dr_ibr_salm@yahoo.com
Ibrahim E. El-Aassy: Nuclear Materials Authority, P.O. Box 530 El Maadi, Cairo, Egypt, e-mail: Ibrahimelaasy4@gmail.com
Abdu A. El-Sayed: Nuclear Materials Authority, P.O. Box 530 El Maadi, Cairo, Egypt, e-mail: Geologyabd6852@gmail.com
Abdullah M. Alzahrai: Department of Civil Engineering, Engineering College, Taif University, P.O. Box 11099, Taif 21944, Saudi Arabia, e-mail: amyalzahrni@tu.edu.sa
El Saeed R. Lasheen: Geology Department, Faculty of Science, Al-Azhar University, P.O. Box 11884, Cairo, Egypt, e-mail: elsaeedlasheen@azhar.edu.eg

1 Introduction

The basement rocks of Sinai represent the northwestern extremity of the Arabian-Nubian Shield (ANS) separated from the main block by the Gulf of Suez and the Gulf of Aqaba. These rocks were formed as a result of complex events of subduction, accretion, and extension during Pan African times [1,2]. The Gabal Serbal area is located in the southwestern part of Sinai Peninsula, between latitudes 28° 32′ and 28° 40′ 43″N and longitudes 33° 34′ and 33° 41′ 30″E (Figure 1). The area under investigation covers about 233 km^2 and is considered a part of the Arabian-Nubian Shield. The Pan-African dike swarms in southwestern Sinai were classified into two swarms: the first (oldest) strikes at 35° and exhibits calc-alkaline chemical properties while the second strikes at 135° and displays transitional to mildly alkaline properties [3]. Geology is considered one of the most important and best sciences in ancient and modern times. It helps discover some of the geological secrets hidden in deep burials and different rocks containing some minerals that have economic feasibility [4]. Dikes are economically significant because they are critical in the formation of world deposits such as tungsten and gold [5,6], and they structurally control the flow and thus the exploration of natural resources such as groundwater and geothermal energy [7,8]. On the other hand, radioactive mineralization linked with red, black, and jasperoid silica veins exhibits apparent brilliant yellow secondary uranium-bearing minerals [9–12].

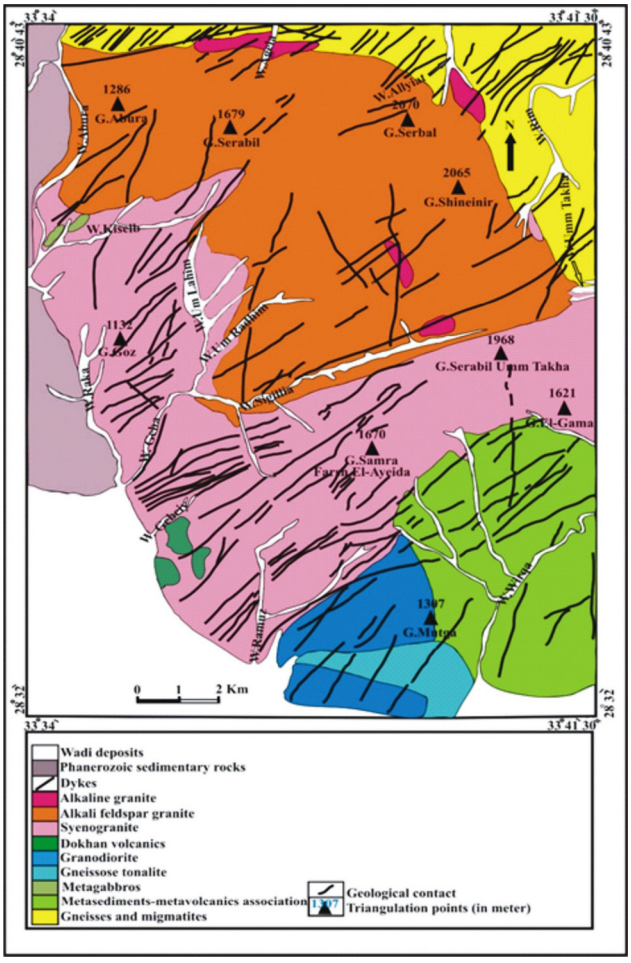

Figure 1: Distribution map of dikes traversing the rock varieties in the G. Serbal area, Southwestern Sinai, Egypt (Kamar [19]).

Dikes may be straight (and parallel to rift zones), curved, or radiating, with the focal point of the swarm understood to designate the core of a magmatic edifice or mantle plume [13], and are often linked with crustal extension [14–16]. It has long been assumed that dike emplacement is somewhat regulated by the regional stress field based on field connections [17,18]. The present study aims to detect the petrography and geochemistry analyses in addition to determine some of the economic mineralization associated with the different dikes at the Gabal Serbal area, Southwestern Sinai, Egypt.

2 Materials and methods

2.1 Geological setting of dikes

The post-granitic dikes of the study area occur either as single dikes or as swarms. These dikes are the product of the most recent episodes of magmatism. They have vertical or steeply sloped bodies that have been injected into all of the preceding strata. Their widths range from 0.5 to 15 m. The dike swarms are more resistant to weathering and erosion than their host. The contacts between dikes and their host rocks are sharp. These dikes are classified into acidic and basic dikes. Acidic dikes are represented by porphyritic dacite, microgranite, granophyre, and alkaline granophyre. Porphyritic dacite dikes are massive and fine-grained with a grayish color. These dikes strike at NE–SW, and N–S. Porphyritic dacite dikes have irregular shapes and their width varies between 0.8 and 2.5 m. They cut the gneisses and migmatites in Wadi Agela and the younger granites in Wadi Gebeiy. Microgranite dikes are massive, porphyritic, and fine-grained with pale red color. They exhibit porphyritic texture, where quartz, plagioclase, and K-feldspar are the phenocrysts. These dikes are vertical and strike at NNE–SSW and N–S. They range between 0.5 and 2.5 m in width and cut the younger granites in Wadi Gebeiy. Granophyre dikes are massive, porphyritic, and fine-grained with a greenish-gray color. Biotite, quartz, K-feldspar, and plagioclase phenocrysts are embedded in a quartz-feldspathic matrix. These dikes are of limited distribution and strike at NE–SW with their widths varying between 0.5 m and 5 m. They cut the gneisses in Wadi Agela and the younger granites in Wadi Abura. Alkaline granophyre dikes are massive, porphyritic, and fine-grained with red color. Quartz, K-feldspar, riebeckite, and plagioclase phenocrysts are embedded in the quartz-feldspathic matrix. These dikes are of limited distribution and strike at NE–SW to ENE–WSW and their widths vary between 1 and 15 m (Figure 2a). They cut the gneisses and migmatites and alkaline granite in Wadi Agela and also the alkali feldspar granite in Wadi Abura. Basic dikes are represented by basalt and dolerite dikes. Basalt dikes are hard, fine-grained with a dark green to grayish-green color. They occur as single or as swarms (Figure 2b). They are marked by negative topography and suffer exfoliation weathering forming onion structures. Basaltic dikes strike NNE–SSW, N–S, and NNW–SSE varying in width from 0.5 to 5 m. Also, the thicker dikes attain a well-pronounced chilled margin against the host rock. They are observed cutting the gneisses and migmatites at Wadis: Agela, Allyiat, Rim, and Um Takha also cutting metasediments–metavolcanic association at Wadi Wirqa. They cut older granites between Wadi Ramuz and Wadi Wirqa. These dikes cut the younger granite at Wadis Geba, Gebeiy, and Abura. Dolerite dikes are medium-grained with dark-green to reddish-brown color. They are marked by negative topography relative to their country rocks. These dikes strike at NNE-SSW

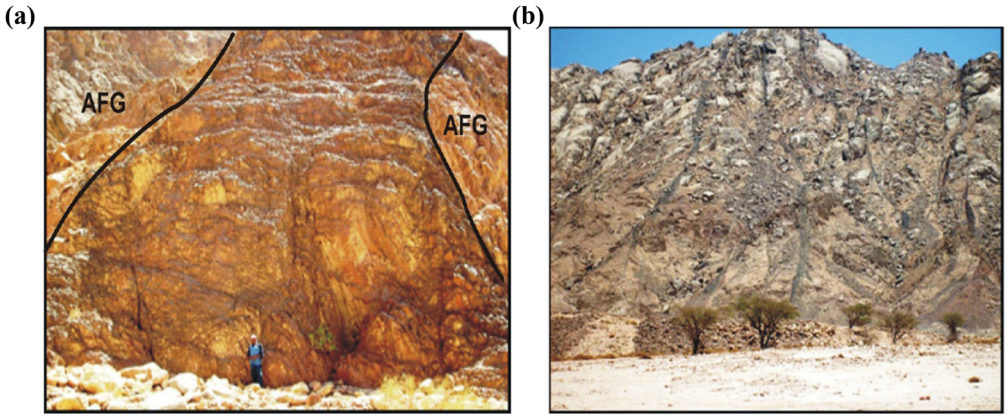

Figure 2: Field photographs showing (a) alkaline granophyre dike cutting alkali feldspar granite (AFG) at Wadi Abura; striking at ENE; and (b) dyke swarms of basalt cutting syenogranite at Wadi Geba; striking at N 65° E.

and NE–SW. They vary in their width between 0.5 and 6 m. The thicker dikes attain a very distinctive chilled margin, where the margin of the dike is fine-grained, and the grain size increases inwards the dyke core. The latter is characterized by porphyritic texture with coarse-grained plagioclase phenocrysts. They cut the gneisses at Wadi Rim: the older granites between Wadi Ramuz and Wadi Wirqa and younger granites at Wadi Geba. One of them cuts the syenogranite at the mouth of Wadi Geba. It exhibits minerals alteration product at its periphery and the contact record high radioactive anomaly. This dike acts as a physical and chemical barrier for the accumulation of radioactive minerals. In the study area, there are about 142 major dikes, and totally, about 278.8 km length was traced and mapped (Figure 1). The directional trend analysis indicates that these dikes exhibit three main trends, namely, N (33–56°) E with tensional regime N (34–57°) W, N (57–76°) E with tensional regime N (14–33°) W, and N (12–32°) E with tensional regime N (58–78°) W regarding their number and length proportions.

2.2 Methods and sample collection

A total of 36 samples were collected from the studied dikes in the assessed region. Chemical analysis was performed on 18 samples from various types of dikes. The samples (about 1 kg) were transferred to the laboratory for analysis. The acquired samples were dried and sieved through a fine mesh (1 mm) (0.256) mm sieve for homologation. To completely dry the samples, they were put in an oven and baked for a day at 100°C. After weighing the samples, they were transported to a 212.6 cm^3 polyethylene measuring cylinder with a 9.5 cm diameter and a 3 cm height. Major oxides and trace elements were detected using the X-ray fluorescence technique. X-ray fluorescence analysis (XRF) is a sophisticated spectroscopic method used to determine a substance's elemental makeup. Numerous elements, from beryllium (Be) through uranium, may be investigated using XRF (U). The X-ray powder diffraction technique collects and analyzes the spectrum produced when the test material is exposed to X-ray radiation. The voltage has been adjusted at 10 kV for light elements, 20–30 kV for medium elements, and 40–50 kV for heavy elements. Additionally, since the environment has a considerable effect on the spectrum when studying light elements, the sample chamber is either evacuated or helium-filled [20–22]. The spectrometer was used to determine the chemical element content of a variety of substances, including those that are solid, powdered, or liquid, as well as those that are deposited on the surface or on filters. Heavy minerals were separated using a heavy liquid (bromoform) separation technique, followed by magnetic fractionation using a Frantz isodynamic separator. The binocular microscope was used to collect the heavy minerals, which were then identified using the environmental scanning electron microscope (ESEM)-energy dispersive X-ray (EDX) approach. All studies were conducted at the Nuclear Materials Authority's Laboratories (NMA).

3 Results

3.1 Petrography of dikes

More than 30 samples of post-granitic dikes were investigated using a polarizing microscope in order to detect their mineralogical and textural relationships. They can be classified into acidic and basic dikes as follows.

3.1.1 Acidic dikes

3.1.1.1 Porphyritic dacite

Porphyritic dacite is composed of plagioclase, quartz, and K-feldspar as essential felsic minerals, whereas biotite and hornblende are mafic minerals. Porphyritic dacite is marked by the porphyritic texture. Plagioclase crystals range in size from euhedral to subhedral (0.8 mm × 2.1 mm) and are composed of oligoclase and andesine (An_{17-36}). It exhibits albite and pericline twinning and has been changed to saussurite (Figure 3a). Occasionally, normal zoning of plagioclase phenocrysts is seen. Quartz is found as 1.2 mm × 2.4 mm subhedral to anhedral phenocrysts and as a fine-grained groundmass. Phenocrysts exhibit excessive extinction as a result of the cataclastic effect. K-Feldspar appears as 1.1 mm × 2.3 mm subhedral phenocrysts and as anhedral fine-grained groundmass. Orthoclase and orthoclase microperthite are the minerals that comprise them. Kaolinization of K-feldspar occurs in stages ranging from partial to total. Biotite occurs in the form of subhedral phenocrysts with dimensions of 0.5 mm × 2.1 mm and as a fine-grained groundmass. It demonstrates partial transformation to chlorite and iron oxides at the crystal borders. Hornblende occurs as 0.5 mm × 1.9 mm subhedral to anhedral phenocrysts. Opaques appear as fine crystals ranging from subhedral to anhedral in conjunction with mafic minerals.

3.1.1.2 Microgranite

Microgranite is composed essentially of quartz, K-feldspar, plagioclase, and biotite as essential minerals, while opaques are accessory minerals. Quartz occurs as euhedral to subhedral phenocrysts (1.1 mm × 2.1 mm) and as fine-grained groundmass. The phenocryst shows weak undulose extinction and corroded edges by the component of the groundmass. K-Feldspar exists as euhedral to subhedral phenocrysts (1.1 mm × 1.9 mm) and as fine-grained groundmass. K-Feldspar is represented by orthoclase and microcline microperthite (Figure 3b). It is sometimes altered to kaolinite and poikilitically quartz and plagioclase. Plagioclase exists as subhedral to anhedral phenocrysts (0.8 mm × 2.1 mm) embedded in fine-grained groundmass forming porphyritic texture. It is of albitic to oligoclase (An_{8-15}) in composition. It shows albite/Carlsbad and pericline twinning and altered to saussurite. Normal zoning of phenocrysts is observed. Biotite occurs as small euhedral to subhedral flakes with the pleochroic formula: X = brown and $Y = Z$ = dark brown. It is altered to chlorite, especially along its cleavage planes. Opaques are represented by fine-grained aggregates associated with biotite.

3.1.1.3 Granophyre dike

It is composed essentially of quartz, K-feldspar, plagioclase, and biotite, while opaques are accessories. Quartz forms subhedral to anhedral crystals and attains 0.3–2.1 mm in length and 0.1 to 0.6 mm in width. Granophyre dike is intergrown with K-feldspar to produce a graphic texture (Figure 3c). K-Feldspar occurs as subhedral to euhedral crystals, ranges from (0.4 mm × 2.50 mm) to (0.2 mm × 0.9 mm) in dimensions, and are represented by perthite and orthoclase perthite and partly altered to kaolinite. Plagioclase forms euhedral to subhedral crystals, and ranges 0.2 mm × 3.5 mm in phenocryst and 0.1 mm × 0.9 in the groundmass. It ranges in composition from oligoclase to andesine (An_{15-34}) and shows zoning and lamellar twinning. Biotite occurs as subhedral to anhedral phenocryst flakes (0.3 × 3.4 mm) with the pleochroic formula X = yellowish-brown and $Y = Z$ = dark brown. It is partly altered to chlorite and iron oxides. Opaques are rare and usually associated with biotite.

3.1.1.4 Alkaline granophyre

Alkaline granophyre is macroscopically hard, massive, and fine-grained with red color. The alkaline granophyre is composed of essentially quartz, K-feldspar, plagioclase, and riebeckite. Opaques are accessories. Quartz forms subhedral to anhedral crystals and attains 0.1–1.9 mm in length and 0.1–0.5 mm in width. Sometimes, quartz intergrow with K-feldspar forming a graphic texture. K-Feldspar occurs as subhedral to euhedral crystals and attains 2.1 mm × 5.5 mm across in phenocryst and 0.1 mm × 0.7 mm across in the groundmass. It is represented by perthite and orthoclase micro perthite and partly altered to kaolinite. Plagioclase is rare and forms euhedral to subhedral crystals 0.2 mm × 3.5 mm in phenocryst and 0.1 × 0.9 in the groundmass. It ranges in composition from oligoclase to andesine (An_{13-38}) and shows zoning and partly altered to saussurite. Riebeckite occurs as subhedral phenocrysts and attains 0.2–3.1 mm in length and 0.3–1.2 mm in width. The pleochroic formula is X = dark blue, Y = light blue, and Z = greenish (Figure 3d). Opaques are rare and usually associated with riebeckite.

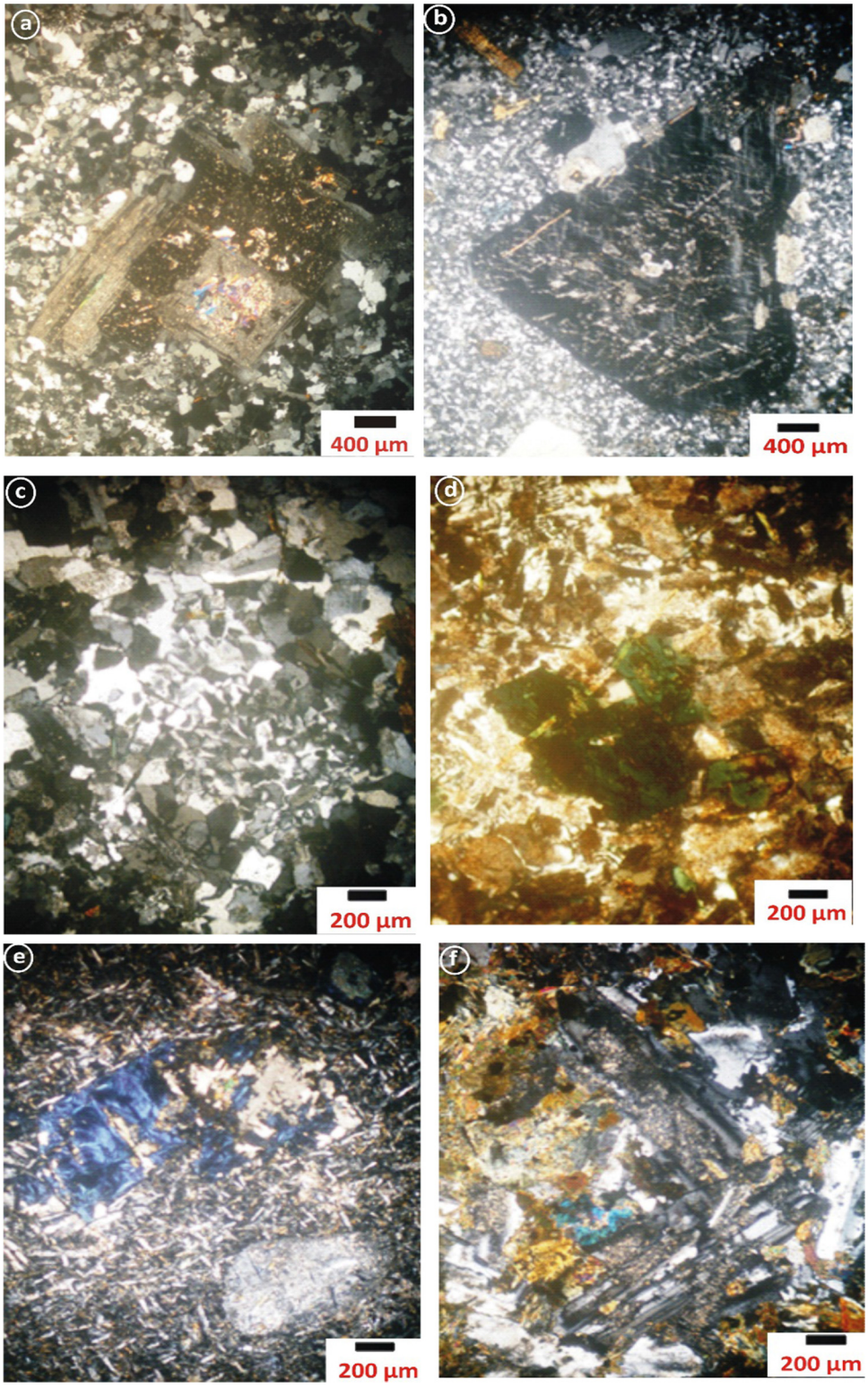

Figure 3: Photomicrographs of (a) porphyritic dacite dike showing pericline twinning in the phenocryst of plagioclase (C.N.); (b) microgranite dike showing phenocryst of microcline micro perthite (C.N.); (c) granophyre dike showing graphic texture (C.N.); (d) alkaline granophyre dike showing riebeckite crystals (C.N.); (e) basaltic dike showing blue pennite type of chlorite and fine-grained lathes plagioclase (C.N.); (f) dolerite dike showing characteristic dolerite and intergranular texture (C.N.).

Table 1: Whole rock (Major and trace elements) analysis of post-granitic dikes of G. Serbal area, Southwestern Sinai, Egypt

Oxides	Basic dikes						Acidic dikes											
	Dolerite			Basalt			Porphyritic dacite			Microgranite			Granophyre			Alkaline granophyre		
	1	2	3	5	8	14	10	11	15	12	13	16	3	6	16	4	7	17
SiO_2	49.9	48.9	49.4	49.85	50.10	49.97	68.9	69.20	69.05	71.52	72.10	71.81	69.97	70.10	70.03	71.86	70.50	71.18
TiO_2	1.86	1.80	1.83	1.50	1.40	1.45	0.55	0.50	0.525	0.36	0.26	0.31	0.12	0.10	0.11	0.25	0.25	0.25
Al_2O_3	13.95	14.10	14.02	14.90	14.80	14.85	13.16	12.85	13.005	13.02	12.90	12.96	14.69	14.20	14.44	13.26	13.32	13.29
$Fe_2O_3{}^t$	9.86	9.95	9.905	9.70	9.60	9.65	3.01	2.80	2.905	3.52	3.10	3.31	2.80	2.50	2.65	2.80	2.90	2.85
MgO	8.30	8.65	8.475	8.83	8.60	8.715	2.75	2.70	2.725	1.12	1.02	1.07	1.28	1.10	1.19	0.43	0.52	0.475
CaO	10.15	10.20	10.17	8.48	8.10	8.29	4.54	4.20	4.37	1.68	1.40	1.54	2.52	2.30	2.41	2.24	2.36	2.3
Na_2O	2.30	2.10	2.2	1.82	1.90	1.86	3.40	3.50	3.45	3.20	3.60	3.4	2.43	2.70	2.565	4.50	4.30	4.4
K_2O	0.75	1.01	0.88	1.09	1.60	1.345	2.36	2.70	2.53	3.40	3.90	3.65	4.74	4.80	4.77	3.30	3.10	3.2
P_2O_5	0.85	0.90	0.875	0.52	0.65	0.585	0.53	0.40	0.465	0.12	0.11	0.115	0.12	0.11	0.115	0.06	0.07	0.065
L.O.I	1.90	1.70	1.8	1.50	1.40	1.45	0.15	0.83	0.49	0.70	0.80	0.75	0.33	0.70	0.515	0.25	0.68	0.465
Total	99.82	99.31	99.56	98.07	98.15	98.11	99.35	99.68	99.515	98.64	99.19	98.915	99.0	98.61	98.80	98.93	98.0	98.46
Trace elements (ppm)																		
Cr	150	214	182	429	390	409.5	32	28	30	42	35	38.5	34	30	32	26	28	27
Ni	86	83	84.5	137	120	128.5	7	6	6.5	11	10	10.5	8	7	7.5	7	9	8
Cu	42	29	35.5	53	50	51.5	11	10	10.5	11	11	11	11	10	10.5	10	11	10.5
Zn	175	419	297	107	101	104	30	25	27.5	37	32	34.5	45	40	42.5	57	51	54
Zr	88	191	139.5	173	180	176.5	157	165	161	222	211	216.5	235	248	241.5	490	432	461
Rb	14	58	36	73	81	77	133	142	137.5	181	192	186.5	122	132	127	172	167	169.5
Y	16	17	16.5	20	21	20.5	24	27	25.5	32	38	35	18	20	19	36	30	33
Ba	280	428	354	586	508	547	178	108	143	103	88	95.5	161	98	129.5	62	70	66
Pb	80	91	85.5	72	60	66	<2	<2	<2	<2	<2	<2	<2	<2	<2	<2	<2	<2
Sr	560	638	599	385	375	380	82	66	74	178	160	169	215	198	206.5	103	125	114
Ga	9	6	7.5	28	22	25	22	20	21	19	15	17	20	18	19	16	18	17
V	255	422	338.5	212	201	206.5	4	4	4	10	8	9	7	6	6.5	8	11	9.5
Nb	<2	<2	<2	<2	<2	<2	3	3	3	8	9	8.5	4	6	5	8	7	7.5

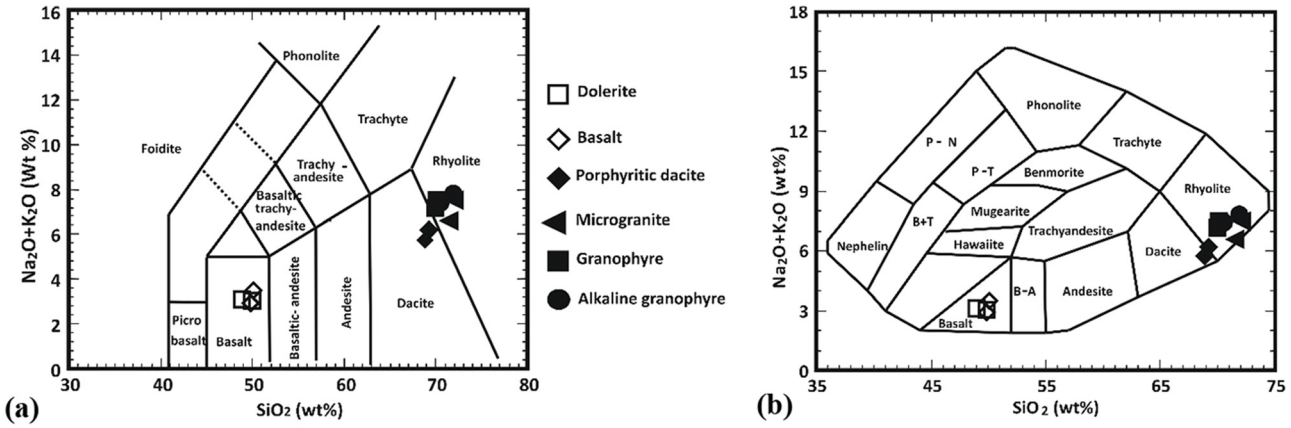

Figure 4: (a) $Na_2O + K_2O$ vs SiO_2 (TAS) diagram for different dikes, after Le Maitre [23]. (b) $Na_2O + K_2O$ vs SiO_2 for the studied dikes (Cox et al. [24]).

3.1.2 Basic dikes

3.1.2.1 Basaltic dike

Basaltic dike is composed of essentially plagioclase phenocrysts and groundmass, hornblende, and pyroxene. Apatite, epidote, chlorite, and opaques are accessory minerals. The intergrowth texture is well developed. Plagioclase occurs as subhedral crystals (0.3 mm × 3.5 mm), phenocrysts, and as groundmass (0.2 mm × 0.5 mm) of labradorite composition (An_{60-68}). Plagioclase crystals show intergranular texture and are associated with calcite, chlorite, and epidote. Partial alteration to saussurite is occasionally present. Hornblende exists as fine-grained euhedral to subhedral crystals. It is altered to chlorite and iron oxides. Pyroxene occurs as subhedral to anhedral crystals and is sometimes altered to tremolite and actinolite. Pyroxene crystals are intergrown with plagioclase laths forming intergranular and subophitic textures. Apatite occurs as elongate euhedral to subhedral crystals, which occur either as independent crystals or incorporated within hornblende and plagioclase. Epidote occurs as an anhedral crystal associated with chlorite. Chlorite occurs as an anhedral phenocryst of pennate type (Figure 3e). Opaques occur as anhedral crystals and are associated with hornblende and pyroxene.

3.1.2.2 Dolerite dike

It composes of plagioclase, hornblende, and pyroxene in addition to trace amounts of biotite, opaques, and sphene. Occasionally, an intergranular texture develops. Plagioclase

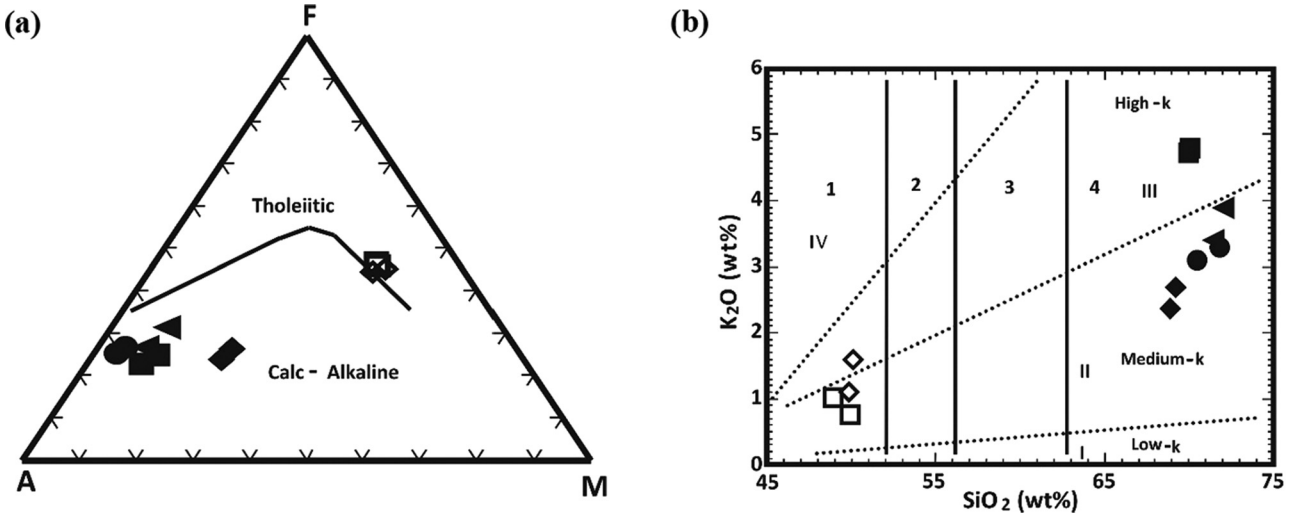

Figure 5: (a) A–F–M diagram for different dikes. Fields, after Irvine and Baragar [25]; symbols as in Figure 4. (b) K_2O vs SiO_2 diagram for different dikes (Peccerillo and Taylor [26]). 1 = basalt, 2 = basalt andesite, 3 = andesite, 4 = dacite and rhyolite, I = arc-tholeiitic, II = calc-alkaline, III = high K-calc-alkaline, and IV = shoshonite; symbols as in Figure 4.

is composed of fine- to medium-grained subhedral to anhedral crystals (1.1 mm × 2.5 mm) of andesine to labradorite ($An_{48–56}$)composition. It contains albite and albite/Carlsbad twinning, as well as saussurite and calcite. Plagioclase laths have an intergranular pyroxene texture. Hornblende crystals range in size from subhedral to anhedral, measuring 1.1 mm × 2.4 mm. It undergoes partial to full transformation into chlorite at the cleavage planes and crystal boundaries and sometimes displays simple merging. Pyroxene is represented by augite and occurs in crystals ranging in size from subhedral to anhedral to 1.1 mm × 2.5 mm. Occasionally, augite crystals develop between plagioclase laths, forming a Doleritic texture (Figure 3f). It demonstrates a diuretic-induced modification of tremolite and actinolite. Biotite occurs as subhedral crystals and undergoes a transformation into chlorite and iron oxides. Opaques form anhedral crystals and are seen in association with mafic elements. Sphene crystallizes in anhedral clusters with plagioclase and ferromagnesian minerals.

3.2 Geochemistry of dikes

Representative samples from the examined dikes were selected and analyzed for major (%) and trace (ppm) elements (Table 1).

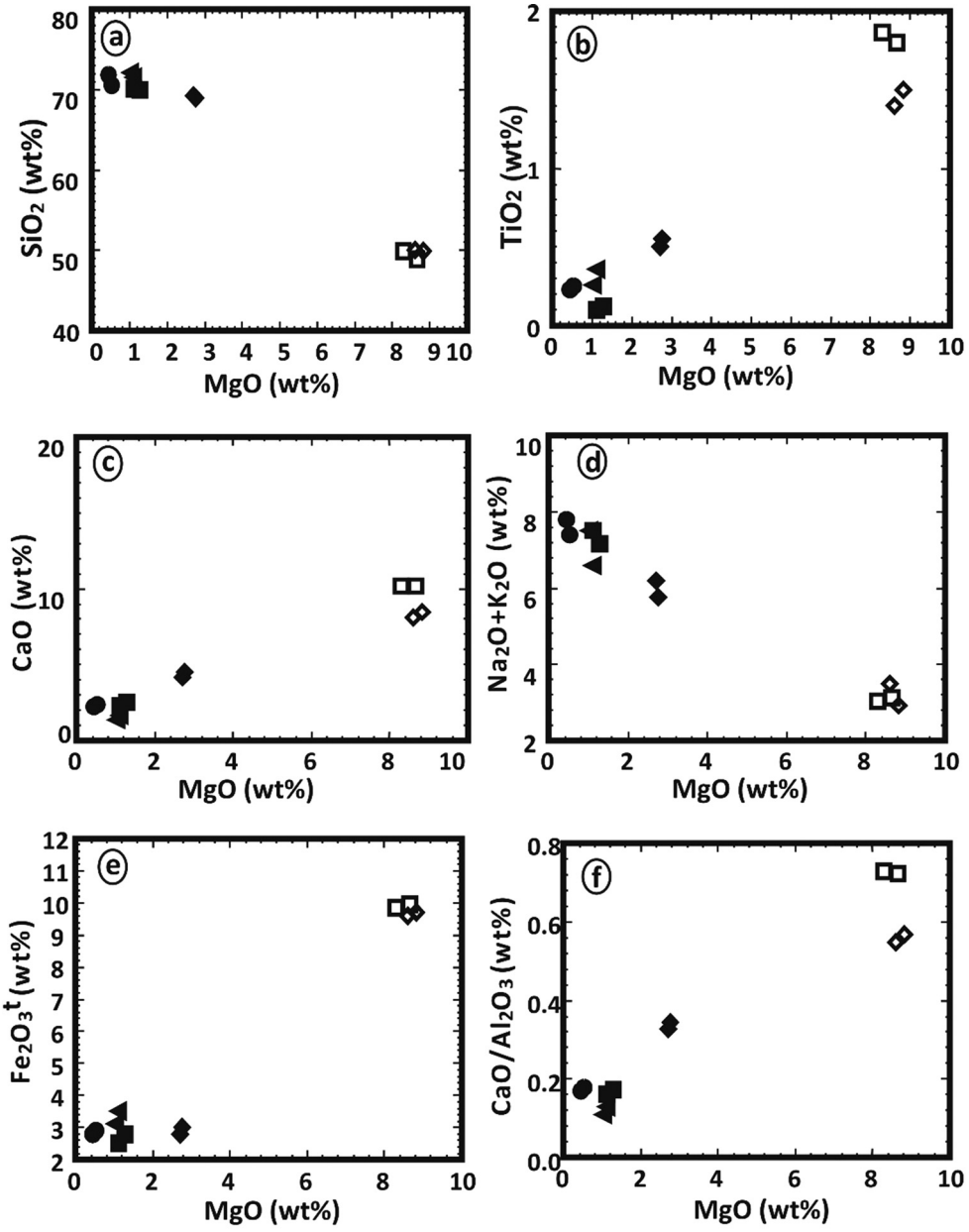

Figure 6: MgO vs (a) SiO_2, (b) TiO_2, (c) CaO, (d) $Na_2O + K_2O$, (e) Fe_2O_3, and (f) CaO/Al_2O_3 for different dikes; symbols as in Figure 4.

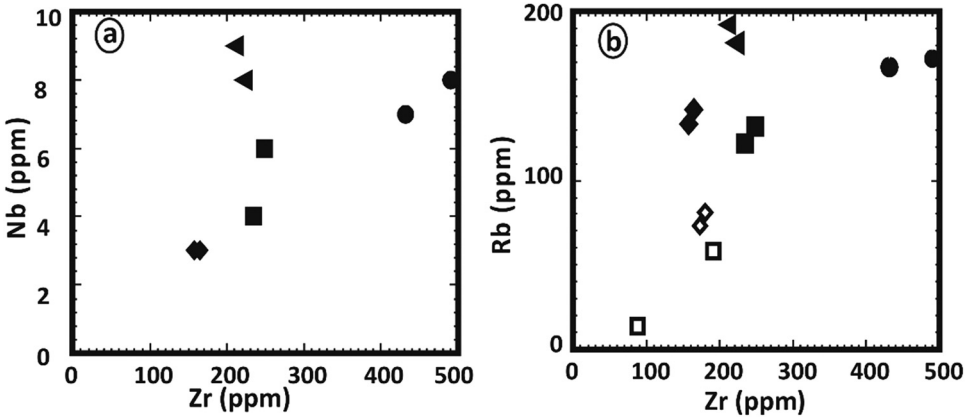

Figure 7: Zr vs (a) Nb, (b) Rb for different dikes; symbols as in Figure 4.

3.2.1 Geochemical classification and characteristics

The studied dikes are classified based on the total alkali–silica diagram (TAS), as suggested by Le Maitre [23] and Cox et al. [24] (Figure 4a and b). The diagrams clarify that the dolerite and basalt samples fall in the basalt field, while porphyritic dacite samples fall in the dacite field. The other acidic dikes (granophyre, alkaline granophyre, and microgranite) samples fall in the rhyolite field.

3.2.2 Magma type and tectonic setting

On the A–F–M ternary diagram (Figure 5), the studied dolerite and basalt samples fall within the tholeiitic field. On the other hand, porphyritic dacite, microgranite, granophyre, and alkaline granophyre samples fall within the calc-alkaline field [25]. To illustrate the potassic nature of the studied dikes, the analyses are plotted on the K_2O vs SiO_2 diagram (Figure 5b) as suggested by Peccerillo and Taylor [26]. It shows that the two samples of dolerite fall in the basalt and medium-*k* calc-alkaline fields, the majority of samples fall in the basalt field, and a few other samples fall in the medium to high calc-alkaline field. The porphyritic dacite, microgranite, and alkaline granophyre samples fall in dacite and rhyolite, medium-*k* calc-alkaline fields. The granophyre samples fall in dacite and rhyolite, high *k*-calc alkaline fields. Binary variation diagrams between MgO and other major oxides (SiO_2, TiO_2, CaO, $Na_2O + K_2O$, Fe_2O_3, CaO/Al_2O_3) are illustrated in (Figure 6) to evaluate the alteration effects on the major oxides' compositions of the investigated dikes. These samples exhibit typical crystallization patterns as seen in these figures. This finding rules out

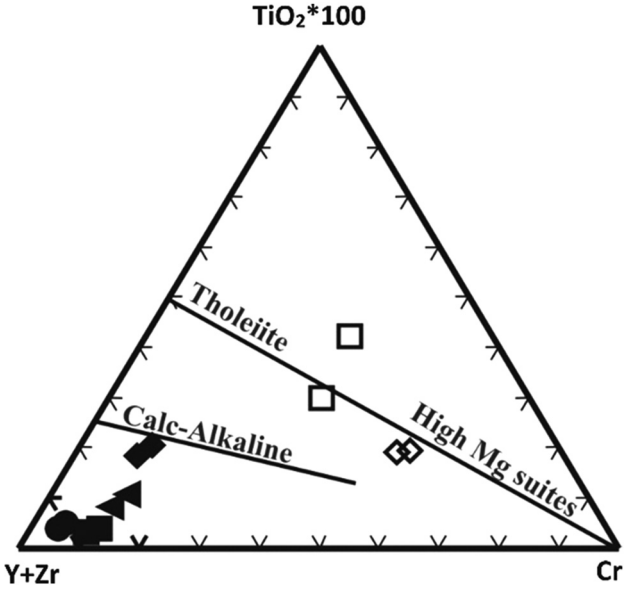

Figure 8: Y + Zr-TiO_2*100–Cr ternary diagram for different dikes, after Davies et al. [27]; symbols as in Figure 4.

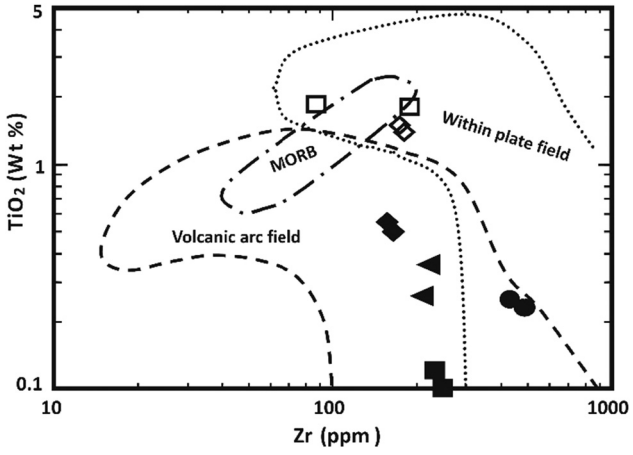

Figure 9: TiO_2 vs Zr diagram for different dikes, after Pearce [28]; symbols as in Figure 4.

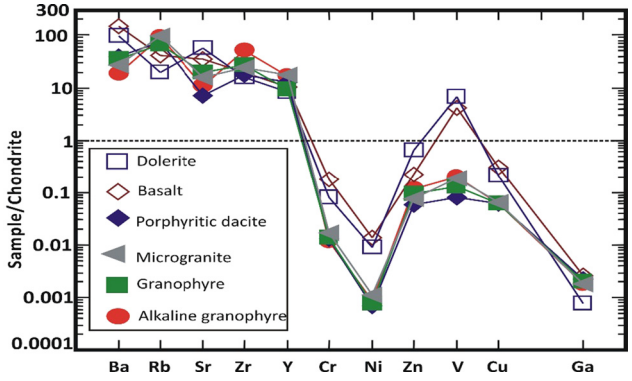

Figure 10: Distribution pattern of trace elements of different dikes normalized to average chondrite (Wood et al. [29]).

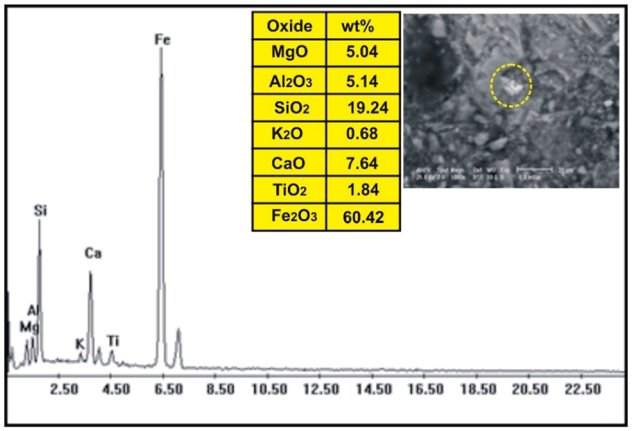

Figure 12: ESEM-EDX analysis of magnetite in basalt dike at Wadi Geba.

the likelihood of these elements being mobilized and implies that these oxides represent magmatic characteristics. Thus, these main oxides may be classified. Zr can be utilized to determine the elemental mobility and to better comprehend magma differentiation. The binary diagrams of Zr–Nb and Zr–Rb (Figure 7) revealed magmatic tendencies with positive relationships between Nb–Zr and Rb–Zr. Thus, trace elements tend to be the least affected by postcrystallization processes and may thus reflect basic properties. Trace elements seem to be more discriminating than large oxides since they are very sensitive to crystal fractionation, rather than to changes in the fundamental composition. The ternary diagram Y + Zr–TiO_2*100–Cr after Davies et al. [27] is constructed to show the original differentiation trend of a magmatic suite because Y and Zr are enriched progressively during fractionation like Na_2O and K_2O (Figure 8a). The TiO_2–Zr diagram (Figure 8b), after Pearce [28], shows that basalt and dolerite fall within the plate field, while porphyritic dacite, microgranite, and granophyre fall in the volcanic arc field.

3.2.3 Petrogenesis

The correlation of the normalized trace elements of the studied dikes with the average of chondrite, after Wood et al. [29] (Figure 9), revealed a depletion in Cr, Ni, Zn, V (except in dolerite and basalt dikes), Cu, and Ga. The other elements Ba, Rb, Sr, Zr, Y, and V (dolerite and basalt dikes) show an enrichment relative to the average of chondrites. The studied dikes are also normalized relative to the primitive mantle values (Figure 10), after Taylor and McLennan [30]. The diagram shows strong enrichment in Ba, Rb, Sr, Zr, and Y, while it shows slight enrichment in Cu (in dolerite and basalt), V (in dolerite and basalt), Zn (in dolerite, basalt, and alkaline granophyre), and Ga. It shows a depletion in Cr, Ni, V (except in dolerite and basalt), and slight depletion in Cu (except dolerite and basalt) and Zn (except dolerite, basalt, and

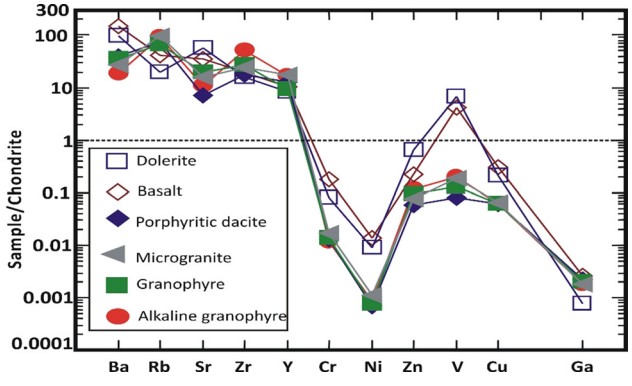

Figure 11: Distribution pattern of trace elements of different dikes normalized to average primitive mantle (Taylor and McLennan [30]).

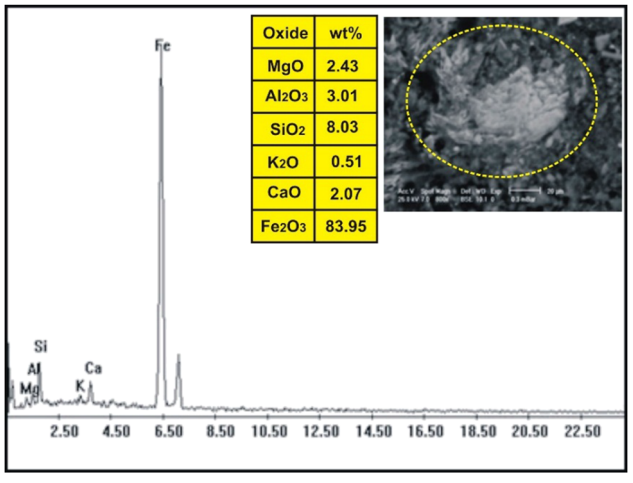

Figure 13: ESEM-EDX analysis of magnetite partially oxidized to hematite in basalt dike at Wadi Geba.

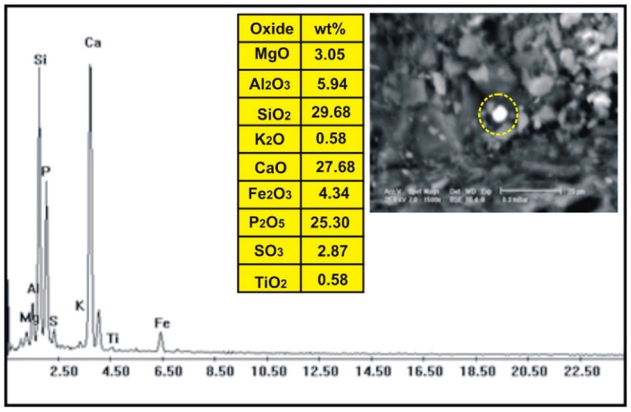

Figure 14: ESEM-EDX analysis of apatite in basalt dike at Wadi Geba.

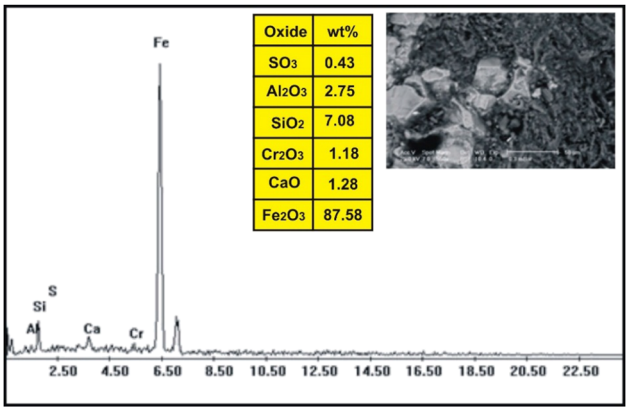

Figure 16: ESEM-EDX analysis of magnetite in dolerite dike at Wadi Geba.

alkaline granophyre) relative to the average of primitive mantle values. Two samples were selected (one for basalt and one for dolerite) for studying the opaque minerals at Wadi Geba. The opaques in basalt are represented by magnetite hematite oxides, apatite, and copper minerals. Magnetite occurs as an anhedral crystal and black with a metallic luster in reflected light. Magnetite was confirmed by the ESEM-EDX technique and contains 60.42% Fe_2O_3 (Figure 11). It is partially or frequently oxidized to hematite (martite). Hematite is steel-gray black with metallic luster in reflected light, with a tendency to a marginal red. Hematite was confirmed by the ESEM-EDX technique and contains 83.95% Fe_2O_3 (Figure 12). Apatite is colorless in a thin section, usually found as minute six-sided prismatic crystals, moderate relief, and weak birefringence. It occurs as an anhedral crystal with a subrounded shape and was confirmed by the ESEM-EDX technique (Figure 13). It contains 25.3% P_2O_5, 29.68% SiO_2, and 27.68% CaO. The copper mineral occurs as an anhedral

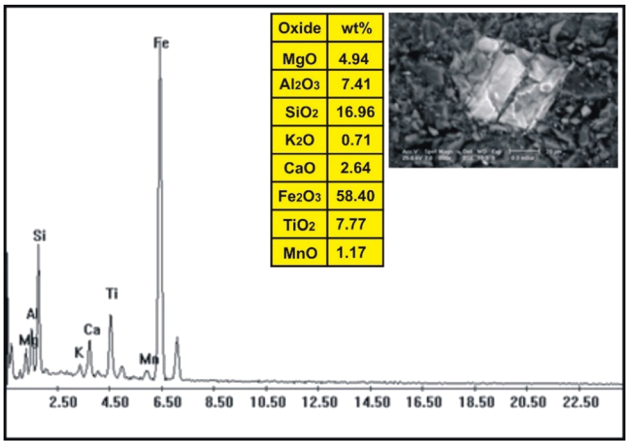

Figure 17: ESEM-EDX analysis of titanomagnetite in dolerite dike at Wadi Geba.

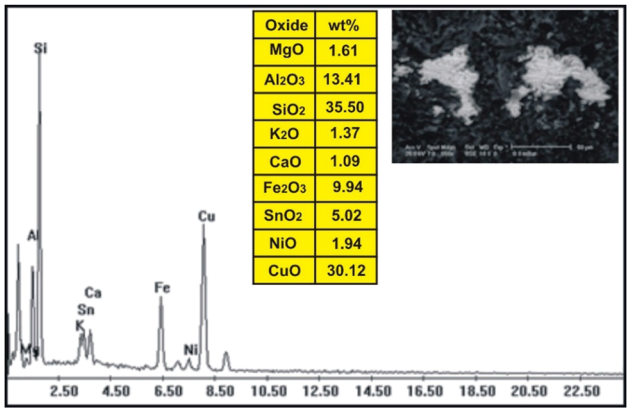

Figure 15: ESEM-EDX analysis of copper minerals in basalt dike at Wadi Geba.

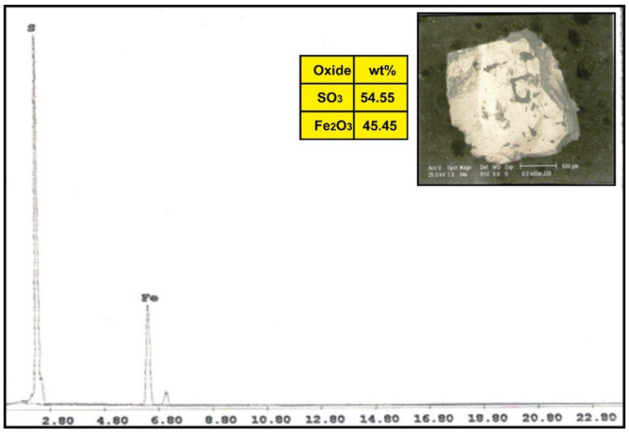

Figure 18: ESEM-EDX analysis of pyrite in dolerite dike at Wadi Geba.

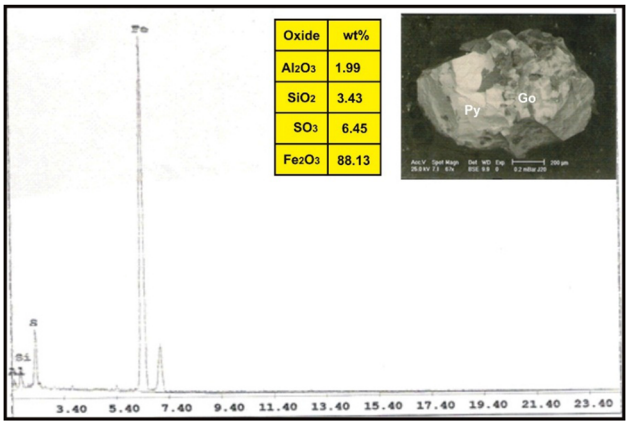

Figure 19: ESEM-EDX analysis of pyrite (Py) replaced by goethite (Go) in dolerite dike at Wadi Geba.

crystal and is confirmed by the ESEM-EDX technique (Figure 14). It contains 30.12% CuO, 9.94% Fe_2O_3, and 35.50% SiO_2. Opaques in dolerite are represented by oxide minerals (magnetite and titanomagnetite) and sulfide minerals (pyrite). Magnetite occurs as a euhedral to subhedral mineral and is confirmed by the ESEM-EDX technique (Figure 15). It contains 87.58% Fe_2O_3. Titanomagnetite is also occurring as euhedral to subhedral minerals. It is less abundant than magnetite and confirmed by the ESEM-EDX technique (Figure 16). It contains 58.40% Fe_2O_3 and 7.77% TiO_2. Sulfide minerals are represented by pyrite, which occurs as cubes and crystalline in the cubic system. It is brass-yellow with a metallic luster in reflected light. It was confirmed by the ESEM-EDX technique (Figure 17) and containing 54.55% SO_3 and 45.45% Fe_2O_3.

Goethite was formed after due to oxidation of pyrite according to the equation

$$\underset{\text{pyrite}}{4FeS_2} + 15O_2 + 2H_2O \rightarrow \underset{\text{goethite}}{4FeO(OH)} + \underset{\text{aqueous}}{8(SO)_3^{-2}}$$

It is yellow to brown in color, greasy to earthy luster, yellowish-brown streak, nonmagnetic unless heated, perfect cleavage in one direction, and partially soluble in hydrochloric acid. Goethite was confirmed by the ESEM-EDX technique (Figure 18) and contains 88.13% Fe_2O_3 and 6.45% SO_3 (Figure 19).

4 Conclusion

The examined area is split by prominent clusters of post-granitic dikes, which create separate and lengthy sub-parallel dike swarms. The directional trend study of post-granitic dikes reveals three principal trends in terms of quantity and length proportions: N (33–56) E with tensional regime N (34–57) W, N (57–76) E with tensional regime N (14–33) W, and N (12–32) E with tensional regime N (58–78) W. These dikes are classified into acidic (porphyritic dacite, microgranite, granophyre, alkaline granophyre) and basic (basalt and dolerite) dikes. The acidic dikes show quite different contents in plagioclase, quartz, alkali felspar, and biotite. On the other hand, basic dikes are represented by pyroxene, hornblende, plagioclase, and iron oxides as well as the opaque minerals relatively more abundant in the basalt dike. The basic dikes have medium *k*-characters, originating from tholeiitic magma and extruded within a plate environment. The acidic dikes have medium to high *k*-characters, originating from calc-alkaline magma and extruded in a volcanic arc environment. The opaques in basalt dikes are represented by magnetite, hematite, apatite, and copper minerals, while dolerite dikes include magnetite, titanomagnetite, pyrite, and goethite minerals.

Acknowledgements: Hamdy A. Awad is funded by a scholarship under the Joint Executive Program between Egypt and Russian Federation.

Funding information: None.

Author contributions: All the authors contributed to writing data curation writing and reviewing a manuscript.

Conflict of interest: The authors declare that they have no conflict of interest.

Ethical approval: The conducted research is not related to either human or animal use.

Data availability statement: All data generated or analyzed during this study are included in this published article.

References

[1] Lasheen ESR, Saleh GM, Khaleal FM, Alwetaishi M. Petrogenesis of neoproterozoic ultramafic rocks, Wadi Ibib–Wadi Shani, South Eastern Desert, Egypt: constraints from whole rock and mineral chemistry. Appl Sci. 2021;11(22):10524.

[2] Saleh GM, Khaleal FM, Lasheen ESR. Geochemistry and paleoweathering of metasediments and pyrite-bearing quartzite during the Neoproterozoic Era, Wadi Ibib-Wadi Suwawrib, South Eastern Desert, Egypt. Arab J Geosci. 2022;15:1–27.

[3] Friz-Töpfer A. Geochemical characterization of Pan-African dyke swarms in southern Sinai: from continental margin to intraplate magmatism. Precambrian Res. 1991;49:281–300.
[4] Awad HAM, Nastavkin AV. Some mechanical and physical studies of granitic rocks in Um Taghir, Eastern Desert, Egypt. J Phys Conf Ser IOP Publishing. 2021; p. 12012.
[5] Rasmussen KL, Lentz DR, Falck H, Pattison DRM. Felsic magmatic phases and the role of late-stage aplitic dykes in the formation of the world-class Cantung Tungsten skarn deposit, Northwest Territories, Canada, Ore. Ore Geol Rev. 2011;41:75–111.
[6] Li L, Li S-R, Santosh M, Li Q, Gu Y, Lü WJ, et al. Dyke swarms and their role in the genesis of world-class gold deposits: insights from the Jiaodong peninsula, China. J Asian Earth Sci. 2016;130:2–22.
[7] Babiker M, Gudmundsson A. Geometry, structure and emplacement of mafic dykes in the Red Sea Hills, Sudan. J African Earth Sci. 2004;38:279–92.
[8] Nukman M, Moeck I. Structural controls on a geothermal system in the Tarutung Basin, north central Sumatra. J Asian Earth Sci. 2013;74:86–96.
[9] Awad HA, Zakaly HMH, Nastavkin AV, El Tohamy AM, El-Taher A. Radioactive mineralizations on granitic rocks and silica veins on shear zone of El-Missikat area, Central Eastern Desert, Egypt. Appl Radiat Isot. 2020:109493.
[10] El Mezayen AM, Heikal MA, El-Feky MG, Shahin HA, Zeid IKA, Lasheen SR. Petrology, geochemistry, radioactivity, and M–W type rare earth element tetrads of El Sela altered granites, south eastern desert, Egypt. Acta Geochim. 2019;38:95–119.
[11] Zakaly HMH, Uosif MAM, Issa SAM, Tekin HO, Madkour H, Tammam M, et al. An extended assessment of natural radioactivity in the sediments of the mid-region of the Egyptian Red Sea coast. Mar Pollut Bull. 2021;171:112658.
[12] Zakaly HM, Uosif MA, Madkour H, Tammam M, Issa S, Elsaman R, et al. Assessment of natural radionuclides and heavy metal concentrations in marine sediments in view of tourism activities in Hurghada city, northern Red Sea. Egypt J Phys Sci. 2019;3:21–47. doi: 10.21315/JPS2019.30.3.3.
[13] Ernst RE, Buchan KL. Giant radiating dyke swarms: their use in identifying pre-Mesozoic large igneous provinces and mantle plumes. Geophys Monogr. 1997;100:297–334.
[14] Marinoni LB. Crustal extension from exposed sheet intrusions: review and method proposal. J Volcanol Geotherm Res. 2001;107:27–46.
[15] Zhang CL, Zou HB. Permian A-type granites in Tarim and western part of Central Asian Orogenic Belt (CAOB): genetically related to a common Permian mantle plume? Lithos. 2013;172:47–60.
[16] Chen N, Dong J, Chen J, Dong C, Shen Z. Geometry and emplacement of the Late Cretaceous mafic dyke swarms on the islands in Zhejiang Province, Southeast China: insights from high-resolution satellite images. J Asian Earth Sci. 2014;79:302–11.
[17] Sibson RH. Brittle-failure controls on maximum sustainable overpressure in different tectonic regimes. Am Assoc Pet Geol Bull. 2003;87:901–8.
[18] Takada A. Variations in magma supply and magma partitioning: the role of tectonic settings. J Volcanol Geotherm Res. 1999;93:93–110.
[19] Khaleal FM, Kamar MS, El-Sherif AM. Geology, geochemistry and radioactivity of the monzogranite Rocks, North Wadi Ghadir, South Eastern Desert, Egypt. Nucl Sci Sci J. 2017;6:71–91. doi: 10.21608/NSSJ.2017.30774.
[20] Dar MA, Uosif MA, Mohamedein LI, Madkour AG, Zakaly HMH. Radiation hazards and the cancer risk assessments in the sediments of Timsah Lake, Egypt. J King Abdulaziz Univ Mar Sci. 2020;30:1–16. doi: 10.4197/Mar.30-1.1.
[21] El-Taher A, Zakaly HMH, Elsaman R. Environmental implications and spatial distribution of natural radionuclides and heavy metals in sediments from four harbours in the Egyptian Red Sea coast. Appl Radiat Isot. 2018;131:13–22. doi: 10.1016/j.apradiso.2017.09.024.
[22] Mostafa MYA, Zakaly HMH, Uosif MAM, Issa SAM, Madkour H, Tammam M. Sediment natural radioactivity and heavy metals assessment from the beaches of Ras-gharib, Red Sea, Egypt. AIP Conference of Proceedings. AIP Publishing LLC AIP Publishing; 2020. p. 020011. doi: 10.1063/5.0032164.
[23] Le Maitre RW. A proposal by the IUGS Subcommission on the Systematics of Igneous Rocks for a chemical classification of volcanic rocks based on the total alkali silica (TAS) diagram: (on behalf of the IUGS Subcommission on the Systematics of Igneous Rocks). Aust J Earth Sci. 1984;31:243–55.
[24] Cox KG, Bell JD, Pankhurst RJ. The Interpretation of Igneous Rocks. London: London University; 1979. p. 450.
[25] Irvine TNJ, Baragar WRA. A guide to the chemical classification of the common volcanic rocks. Can J Earth Sci. 1971;8:523–48.
[26] Peccerillo A, Taylor SR. Geochemistry of Eocene calc-alkaline volcanic rocks from the Kastamonu area, northern Turkey. Contrib Mineral Petrol. 1976;58:63–81.
[27] Davies JF, Grant RWE, Whitehead RES. Immobile trace elements and Archean volcanic stratigraphy in the Timmins mining area, Ontario. Can J Earth Sci. 1979;16:305–11.
[28] Pearce JA. Geochemical evidence for the genesis and eruptive setting of lavas from Tethyan ophiolites. Proceedings International Ophiolite Symposium, Cyprus 1979. Cyprus: Ministry of Agriculture and Natural Resources; 1980. p. 261–72.
[29] Wood DA, Tarney J, Varet J, Saunders AD, Bougault H, Joron JL, et al. Geochemistry of basalts drilled in the North Atlantic by IPOD Leg 49: implications for mantle heterogeneity. Earth Planet Sci Lett. 1979;42:77–97.
[30] Taylor SR, McLennan SM. The continental crust: its composition and evolution. Oxford: Blackwell; 1985. p. 1–312.